



EUROPEAN ORGANIZATION FOR NUCLEAR RESEARCH

CERN/EP 81-131
19 October 1981

CHARM PARTICLE PRODUCTION IN 360 GeV π^-p AND 360 GeV pp INTERACTIONS

LEBC EHS Collaboration

Amsterdam¹-Brussels²-CERN³-Madrid⁴-Mons⁵-Nijmegen⁶-Oxford⁷-Padova⁸-Paris⁹-
Rome¹⁰-Rutherford Lab¹¹-Serpuukhov¹²-Stockholm¹³-Strasbourg¹⁴-Torino¹⁵-
Trieste¹⁶-Vienna^{17*} Collaboration

M. Aguilar-Benitez³, W. Allison⁷, P. Bagnaia¹⁰, B. Baldo^{10†}, L. Barone¹⁰,
W. Bartl¹⁷, V. Baseeva¹², A. Bergier³, A. Bettini⁸, R. Bizzarri¹⁰,
M. Boratav⁹, G. Borreani¹⁵, F. Bruyant³, E. Castelli¹⁶, P. Checchia¹⁶,
P. Chliapnikov¹², G. Ciapetti¹⁰, G. Cooremans-Bertrand², D. Crennell¹¹,
M. Cresti⁸, F. Crijns⁶, H. Dibon¹⁷, E. Di Capua¹⁰, C. Dionisi¹⁰, J. Dolbeau⁹,
J. Duboc⁹, J. Dumarchez³, F. Etienne¹⁴, A. Ferrando⁴, C. Fisher¹¹,
Y. Fisjak¹², R. Fruhwirth³, U. Gasparini⁸, L. Gatignon⁶, S. Gentile³,
P. Girtler¹⁷, F. Grard⁵, J. Hanton⁵, F. Hartjes¹, P. Herquet⁵, S. Holmgren¹³,
J. Hrubec¹⁷, P. Hughes⁷, E. Johansson³, J. Kesteman⁵, A. Kholodenko¹²,
E. Kistenev¹², S. Kitamura³, W. Kittel⁶, N. Kurtz¹⁴, P. Ladron de Guevara⁴,
J. Lemonne², J. Lesceux⁵, H. Leutz³, L. Lyons⁷, P. Loverre¹⁰, F. Marchetto¹⁵,
M. Markytan¹⁷, F. Marzano¹⁰, M. Mazzucato⁸, E. Menichetti¹⁵,
M. Michalon-Mentzer¹⁴, A. Michalon¹⁴, N. Minaev¹², T. Moa³, L. Montanet³,
G. Neuhofer¹⁷, H. Nguyen⁹, S. Nilsson¹³, L. Peruzzo⁸, P. Pilette⁵, G. Piredda¹⁰,
A. Poppleton³, P. Poropat¹⁶, P. Porth¹⁷, M. Regler¹⁷, S. Reucroft³,
G. Rinaudo¹⁵, L. Robb¹¹, P. Rossi⁸, J. Rubio⁴, G. Sartori⁸, M. Sessa¹⁶,
A. Stergiou⁶, V. Stopchenko¹², A. Subramanian³, S. Tavernier², O. Tchikilev³,
D. Toet¹, M. Touboul⁹, A. Touchard⁹, C. Troncon¹⁶, M. Van Immerseel²,
L. Ventura⁸, P. Vilain², J. Wickens², V. Yarba¹², T. Yiou⁹, D. Zanello¹⁰,
L. Zanello¹⁰, G. Zholobov¹², P. Zotto⁸ and G. Zumerle³

Presented at the International Conference on High Energy Physics
9 - 15 July, Lisbon, Portugal

* Supported in part by Österreichischer Forschungsrat.

† We would like to record our sincere appreciation for the work of Bruno Baldo of Rome who contributed much to the success of the experiment. Unfortunately he died a few weeks before the Lisbon meeting after a short illness.

ABSTRACT

Results are presented on charm particle production from an initial analysis of data taken with the European Hybrid Spectrometer and the high resolution hydrogen bubble chamber LEBC operating in both 360 GeV π^- and 360 GeV proton beams. From a total of 19 fully reconstructed decays, the D^\pm and D^0 lifetimes are found to be

$$\tau(D^\pm) = 8.0^{+4.9}_{-2.4} \times 10^{-13} \text{ s}, \quad \tau(D^0) = 3.2^{+2.2}_{-1.0} \times 10^{-13} \text{ s}.$$

One F meson is observed in association with a D meson. In 360 GeV π^-p interactions D mesons are observed with a production distribution $dN/dx_F \propto (1 - x_F)^n$ with $n = 3.2 \pm 1.0$ for $x_F \geq 0.0$. The inclusive π^-p cross section for D^\pm with $x_F \geq 0.0$ is found to be $11 \pm 5 \text{ } \mu\text{b}$. A clear rapidity correlation exists between charm meson pairs. The mean $\langle p_T \rangle$ is found to be 780 MeV/c. At the present level of statistics no differences between πp and pp charm production characteristics can be seen.

The high resolution hydrogen bubble chamber LEBC has been used in association with the European Hybrid Spectrometer (EHS) to study the production and decay characteristics of charm particles produced in hadronic interactions at the SPS. Data were taken using an interaction trigger, with incident 360 GeV π^- (~ 400 K pictures corresponding to 10 ev/ μb) and 360 GeV protons (650 K pictures ~ 12 ev/ μb). We report here results based on an initial analysis of about 50% of the pion data and about 15% of the proton data.

1. DETAILS OF THE DATA TAKING

The layout of the version of the apparatus used in this experiment is shown in fig. 1 and described in detail elsewhere [1]. It can be considered in five parts: (a) vertex detection; (b) triggering; (c) charged particle momentum analysis; (d) gamma detection and measurement; (e) charged particle identification.

(a) Vertex detection

The bubble chamber, LEBC, is 20 cm in diameter and 4 cm deep and was constructed entirely of LEXAN. The bright field scotchlite optical system gave two views of each event (stereo angle 16°) with resolution $\sim 35 \mu\text{m}$. The optical depth of field was ~ 5 mm with two 180 mm Schneider Componon lenses operated at F/11, and space to film demagnification of 3.25. The chamber was filled with hydrogen and expansion was achieved with a piston pushing against the Scotchlite coated lexan membrane at the rear of the chamber. Operation was at 33 Hz with pressure and temperature conditions chosen to give a bubble density $\sim 80/\text{cm}$. The flash was triggered with a delay $\sim 300 \mu\text{s}$ to give $\sim 40\text{-}50 \mu\text{m}$ diameter bubbles. A typical picture is shown in fig. 2 and a detailed description of the construction and operation of LEBC is given in [2]. Residuals of straight line fits to measured points on tracks in the chamber are $\sim 6 \mu\text{m}$ in space.

(b) Triggering

The interaction trigger, shown in fig. 3, is defined by the logic $T_1 \cdot (L+R) \cdot T_3 \cdot \bar{V} \cdot T_4 \cdot T_5$, corresponding to an incoming beam particle, within the central 2 mm of the optical depth of field, in coincidence with at least

two particles in the downstream counters T_4 and T_5 . The observed trigger cross sections for this arrangement are ~ 16 mb for incident pions and ~ 22 mb for incident protons.

A beam kicker magnet was used to remove particles during the pressure drop of the chamber expansion and triggers were accepted from interactions within a sensitive gate set at 600 μ sec around the minimum of the expansion curve. Approximately 10-12 pictures were taken for each SPS 2 s flat top and the associated spectrometer information was written on tape. About 40% of the pictures have an event within the fiducial region defined for primary interactions (~ 13 cm of liquid hydrogen).

(c) Momentum Analysis

The spectrometer magnet M1 (1.5 T.m) situated 1.8 m from the centre of LEBC has useful aperture ~ 100 cm vertical (bend plane) \times 40 cm horizontal. The first stage of the momentum analysis is provided by the wire/drift chambers W2 (6 planes), D4, D2 and D3 (each of 4 planes). An inclined proportional chamber [3] was installed immediately downstream of magnet M1 for the latter part of the data taking. Secondary particles having momentum > 20 GeV/c were accepted by the second stage of momentum analysis provided by the magnet M2 (3 T.m) and the chambers D1 and D5 (each of 4 planes). The acceptance of the spectrometer for the decay products of D mesons as a function of x_F , defined as usual by $x_F = 2p^*/\sqrt{s}$, is shown in fig. 4. Spectrometer track residuals are typically $\lesssim 300$ μ m and $\Delta p/p \lesssim 1\%$.

A detailed description of the design and optimisation of the drift chamber geometry is given in [4].

The track reconstruction efficiency between bubble chamber and spectrometer, for tracks within the acceptance of M1, is $\sim 90\%$.

To check the reconstruction through the spectrometer a sample of strange particle decays have been studied. The result of mass determinations for K^0 and Λ^0 , ($\bar{\Lambda}^0$) fits is shown in fig. 5. The mass resolution (r.m.s.) for K^0 decays is typically ~ 5 MeV/c² and for Λ^0 decays ~ 4 MeV/c².

(d) Gamma detection

Gammas are detected by the two lead glass calorimeters IGD and FGD (Intermediate Gamma Detector and Forward Gamma Detector, respectively). In principle all photons passing through the aperture of M1 are detected, however we have a small loss because the centre of LEBC is downstream of the designed spectrometer vertex detector. Photons are measured with energy (FWHM) and angular resolution (RMS) given by

$$\frac{\Delta E}{E} = \left(\frac{15}{\sqrt{E}} + 2\% \right) ; \quad \Delta\phi \sim 0.4 \text{ mr} \quad (\text{IGD})$$
$$\frac{\Delta E}{E} = \left(\frac{10}{\sqrt{E}} + 2\% \right) ; \quad \Delta\phi \sim 0.1 \text{ mr} \quad (\text{FGD})$$

E is in GeV. Fig. 6 shows typical $\gamma\gamma$ effective mass distributions. A clear π^0 peak is observed with width $\approx 20 \text{ MeV}/c^2$ (FWHM). A description of the design and operation of the gamma detection system can be found in [5].

(e) Particle identification

The prototype pictorial drift chamber ISIS1 [6] was operated in the first lever arm. The number of active sense wires (~ 50) gave an ionisation resolution typically $\sim 18\%$ (FWHM) in the 80% argon, 20% CO_2 mixture. The relativistic rise in this gas mixture is 55%. Only limited particle identification information is therefore available.

Electron identification is relatively good in ISIS1, and can also be achieved by comparing the spectrometer momentum measurement of a charged particle with the energy deposited in the lead glass calorimeters.

The spatial track information from ISIS1 has proved to be of considerable value in removing ambiguities occurring in complex events with many tracks in the spectrometer. The two track resolution is $\sim 12 \text{ mm}$ and the r.m.s. mismatch between ISIS1 and the rest of the spectrometer is $\sim 4 \text{ mm}$ in position and $\sim 5 \text{ mr}$ in angle.

2. THE SELECTION OF CHARM CANDIDATES

We report here the initial results of scanning and measuring the first 300 K pictures, corresponding to 5.0 ev/ μ b of the pion exposure and 1.7 ev/ μ b of the proton exposure.

All events were studied using dual magnification scan tables (with, approximately, x15 for event location and x40 for a detailed study of the vertex and the forward cone). The upstream wire chambers U1 and U3 were used to give a scan table coordinate prediction for the beam track giving the trigger and hence corresponding to an interaction having associated spectrometer information on tape. Events showing evidence of secondary activity in the chamber were recorded and classified into the following categories: C_n (n prong charged decay); V_n (n prong neutral decay); G (gamma); X_n (\geq n prong activity with an unclear vertex - usually obscured by overlapping tracks in the forward cone). Secondary interactions in the hydrogen were readily identified and removed from the sample on the basis of prong count. Two independent scans were made followed by a physicist check.

Following the analysis described elsewhere [7,8], candidates for charm decay are selected using the transverse decay length x and decay length L defined in fig. 7. The decay vertices of particles having $p_T <$ rest mass and proper lifetime $< 2.10^{-12}$ s will lie within 0.06 cm of the beam direction independent of the longitudinal momentum^(*).

We report here the results of measurement and reconstruction made on a sample of events defined as follows:

(a) Events having any two decays within a box defined by $x < 0.06$ cm.

or

(*) $x = L \sin \theta_p$ where L is the decay length and θ_p the production angle $x = (p/m) \sin \theta_p \cdot \tau c = (p_T/m) \tau c$; hence for $p_T < m$ and $\tau < 2.10^{-12}$ s we have $x < 0.06$ cm.

- (b) Single decays having a characteristic charm-type topology such as C3, C5, V4, etc.

Thus we have studied a selected sample of events which topologically have a high probability of containing charm decays.

A summary of the scanning information is given in table 1.

3. RECONSTRUCTED CHARM DECAYS

Table 1 gives a summary of all measured events in the characteristic charm topologies defined in the previous section and table 2 summarises all events identified as containing a reconstructed charm decay. This represents our sample at this stage for lifetime and production mechanism analysis. We have six events in which a charm pair has been reconstructed and eight events in which a single decay has been reconstructed. Of these single charm events six have a second at present unidentified decay.

To be included in the sample presented here we require:

- (a) A charm topology (as defined in sect. 2) confirmed by a careful scrutiny of the event to remove any questions concerning possible topological uncertainties. This involves, for example, a search for very short proton recoils or lost tracks in prong counting, etc.;
- (b) That no fit exists within 4σ to any strange particle interpretation;
- (c) That an acceptable interpretation exists in terms of a charm decay. A decay is kinematically fully constrained (NDF = 3) when all of the charged decay products are measured in the spectrometer and all of the neutrals are detected in IGD or FGD. If one or two of the charged particle momenta are missing the decay still has a constrained mass solution (NDF = 2 or 1). Of the 20 decays reported here 15 are fully constrained, 4 have one missing momentum (NDF = 2) and one has two missing momenta (NDF = 1).

Fig. 8(a) shows the mass distribution for events interpreted as D^\pm decays. The Cabibbo preferred decay ($D^\pm \rightarrow K^\mp n\pi$; $n = 1, 2, 3\dots$) is shown hatched and it is significant that in all but one event this assignment gives a good D mass. In general, the Cabibbo unfavoured assignment would not give a good D mass. Fig. 8(b) shows the events of fig. 8(a) but with a $K^+K^-\pi^\pm$ mass assignment. It is clear that the F/D ambiguity is minimal in these data. Fig. 8(c) shows the D^0 mass distribution, again the Cabibbo preferred hypothesis gives a good D mass. The mass resolution is typically $\lesssim 10$ MeV/c² for decays without neutrals and $\lesssim 20$ MeV/c² for decays with neutrals. The mean observed decay multiplicity is 4.0 ± 0.5 for D^0 decays and 3.6 ± 0.9 for D^\pm decays.

4. LIFETIME DETERMINATIONS

The individual observed lifetimes for all reconstructed decays are given in table 2. Event number 10 is interesting since it is a reconstructed pair, one of which is an anomalously long lived D^0 . Topologically it is a two prong V^0 in association with a clear C3 D^- decay. Using a reconstructed π^0 from the gamma detectors a good interpretation is obtained to a $D^0 \rightarrow K^-\pi^+\pi^0$ decay. Taken alone, the V^0 gives a poor fit to a $K^0 \rightarrow \pi^+\pi^-$ decay ($m_{\pi\pi} = 512 \pm 3$ MeV/c²) if not constrained to come from the production vertex. The lifetime for the D^0 interpretation is 3.1×10^{-12} s. It is excluded from the following lifetime analysis since it is inconsistent with the remaining D^0 decays and the interpretation in terms of a single lifetime.

The uncorrected mean lifetimes for all the D^\pm decays and all the D^0 decays are 10.3×10^{-13} s and 3.9×10^{-13} s, respectively. To obtain the best estimate for the mean lifetime for D^\pm and D^0 we have corrected the observed lifetimes by subtracting from each observation the minimum lifetime that could have been detected in that event. We have

$$\frac{c\langle\tau\rangle}{m} = \frac{1}{N} \sum_{i=1}^N \frac{l_i - l_i^{\min}}{p_i}$$

where l_i is the actual decay length for a particle of momentum p_i and

ℓ_i^{\min} is the minimum decay length that would have been detected. We have used only the fully constrained decays in the following analysis since there exists, in principle, the possibility of a reconstruction bias against short lifetimes for the remaining events. In practice the inclusion or exclusion of the four non-fully constrained decays does not change the estimate of the lifetime within the errors.

For charged decays into three prongs the minimum length ℓ_i^{\min} is estimated using the criterion that the event would be found provided that the maximum impact parameter y_{\max} defined in fig. 7, exceeds 100 μm . The impact parameter scales directly with the lifetime so that the minimum detectable lifetime in a given event is found by multiplying the observed lifetime by $100/y_{\max}$. The mean lifetime for charged D mesons is found to be

$$\tau(D^\pm) = 8.0^{+4.9}_{-2.4} \times 10^{-13} \text{ s.} \quad (7 \text{ decays})$$

Fig. 9(a) shows a log linear plot of the D^\pm corrected lifetimes. The solid straight line corresponds to the value of 8.0×10^{-13} s given above.

For neutral D mesons we find that the decays are topologically clear if there exists a gap of at least 1 mm between the production and the decay vertex. For the purpose of estimating the correction to the D^0 lifetime we therefore assume a fixed ℓ_{\min} of 1 mm. Applying the above analysis we find

$$\tau(D^0) = 3.2^{+2.2}_{-1.0} \times 10^{-13} \text{ s} \quad (6 \text{ decays})$$

Fig. 9(b) shows the D^0 lifetime distribution. The solid straight line corresponds to the above best estimate. Note that event number 4 in table 2 was previously reported in ref. [8]. It is interesting to note that, including the anomalous event mentioned earlier there are three relatively long lived events in the D^0 sample. Clearly more statistics are required to settle the D^0 lifetime question.

Because of the complexity of the events the above correction factors are only approximate, however it is clear that at this level of statistics

second order corrections are certainly negligible since these first order considerations do not significantly change the lifetime estimate from the raw mean.

The F decay has a lifetime of $4.21 \pm 0.16 \times 10^{-13}$ s.

5. PRODUCTION MECHANISM AND CROSS SECTION ESTIMATES

In table 2 we give the value of x_F for each reconstructed decay. To determine the physical distribution in x_F we give to each event a weight depending on the spectrometer acceptance for the particular decay mode detected and the detection efficiency at the film scanning stage. The spectrometer acceptance is very low for $x_F < 0$ and therefore in the following we will discuss only forward production with the events weighted by the inverse of the acceptance for the appropriate x_F value. The average weight from the spectrometer acceptance is 1.3.

For charged decays the detection at the scanning stage depends only on the maximum impact parameter y_{\max} being greater than $100 \mu\text{m}$. Since y_{\max} is independent of the production kinematics the x_F distribution must only be corrected for the spectrometer acceptance. The average total weight per event used in the cross section estimate given below is ~ 2.1 for a mean lifetime of 8×10^{-13} s.

For neutral decays the cut in length, $l_{\min} = 1 \text{ mm}$ gives a scanning efficiency weight to the x_F distribution which depends on the lifetime. The correction to the observed x_F distribution for D^0 's therefore depends on the lifetime. Assuming a lifetime $\tau(D^0) = 3.0 \times 10^{-13}$ s the average weight for the decay modes observed, folding in the spectrometer acceptance is again ~ 2.1 . The D^0 sample, however, is subject to additional scanning losses which do not depend on x_F . This sample is therefore not used to estimate a cross section.

Because of the limited statistics in the proton sample we discuss here only the x_F distribution for D mesons observed in the 360 GeV π^- interactions. The weighted x_F distribution for the total $\pi^- p$ charm

sample is shown in fig. 10(b). To obtain reasonable statistics we add the D^\pm and the D^0 distributions together; the D^0 decays are hatched. This distribution is consistent with a form

$$\frac{dN}{dx_F} \propto (1 - x_F)^n \text{ with } n = 3.2 \pm 1.0 \text{ for } x_F \geq 0.0$$

In fig. 11(a) we show the centre of mass rapidity values for pair events individually and for single decay events taken together in fig. 11(b). It is interesting that the charm pairs are closely correlated in rapidity with the exception of one event (number 6, with $\Delta y^* = 2.3$) which is the only pair containing a D^+ meson from the incident π^- beam. The mean rapidity gap for all other pairs is $\langle \Delta y^* \rangle = 0.4$. Event number 5 is interesting because all of the incident energy can be accounted for in the final state particles; a D^- , a slow Λ^0 (~ 1 GeV/c) a π^+ and two π^0 's. The π^+ , which has a barely detectable kink close to the origin, together with one π^0 gives an F^+ mass; an isospin disfavoured decay mode. The event is still under study to resolve an ambiguity in the π^0 reconstruction and will certainly be reported again later.

The transverse momentum distribution for all charm mesons is shown in fig. 12. The mean value of p_T is 0.78 GeV/c.

From the six fitted C3 decays in our π^-p sample, we can estimate the inclusive D^\pm cross section with $x_F \geq 0$ for $\pi^-p \rightarrow D^\pm + \text{anything}$ at 360 GeV. The 198 000 pictures analyzed correspond to a sensitivity of 5 events/ μb and therefore our six events give a cross section of 1.2 μb . This has to be multiplied by the following correction factors:

- 1.9 to take into account the other C3 decays in the sample which do not fit a strange particle decay but have not yet been completely analyzed.
- A weight calculated per event for the spectrometer acceptance and the scanning visibility for the observed decay mode. The mean weight is ~ 2.1 .

The resulting cross section for charm C3 decays is then 4.8 μb . Assuming a branching ratio [10] $D^\pm \rightarrow 3 \text{ prong}/D^\pm \rightarrow \text{all} = 0.45$ we have

$$\sigma(D^{\pm}) = 11 \pm 5 \text{ } \mu\text{b at } 360 \text{ GeV/c for } x_F \geq 0.0$$

Note that of the six decays observed in this region five are D^- .

A similar determination for D^0 and \bar{D}^0 is at present affected by larger inaccuracies since we did not yet completely analyze all V2 topologies. The data are at this stage, however, compatible with equal D^{\pm} and D^0 inclusive cross sections.

The weighted x_F distribution for the three D decays from the pp sample is shown in fig. 10(c). The absence of a clear Λ_c^+ decay in the proton data argues against a large diffractive Λ_c^+ cross section. At this stage in the analysis however we are sensitive only to the $K^- p \pi^+ n \pi^0$ decay modes ($\sim 33\%$ efficiency at $x_F > 0$ for $\sim 2 \times 10^{-13}$ s lifetime). The reconstruction of Λ^0 decays downstream of the bubble chamber should be possible and hence provide sensitivity to the $\Lambda^0 n \pi^0$ decay modes at a later stage in the analysis. We therefore defer giving any limit on Λ_c production until a larger sample of the proton data has been analysed and the overall detection efficiency for Λ_c is better understood.

6. CONCLUSIONS

This initial study of charm particle production in 360 GeV/c π^-p and pp interactions has yielded 20 fully reconstructed charm meson decays with the following properties:

(a) Lifetimes:

$$\tau(D^{\pm}) = (8.0^{+4.9}_{-2.4}) \times 10^{-13} \text{ s}$$

$$\tau(D^0) = (3.2^{+2.2}_{-1.0}) \times 10^{-13} \text{ s}$$

(b) Production characteristics in π^-p at 360 GeV

$$\frac{dN}{dx_F} \propto (1 - x_F)^n \text{ with } n = 3.2 \pm 1.0, \text{ for } x_F \geq 0.0$$

$$\langle p_T \rangle = 780 \text{ MeV/c}$$

Average charm pair rapidity gap, $\langle \Delta y \rangle^* = 0.4$.

(c) Inclusive cross sections for π^-p at 360 GeV ($x_F \geq 0.0$),

$$\sigma(D^\pm) = 11 \pm 5 \mu\text{b}$$

REFERENCES

- [1] LEBC-EHS Collaboration, NA16 Experimental Details, to be submitted to Nucl. Instr. and Meth. (1981).
- [2] J.L. Benichou et al., to be submitted to Nucl. Instr. and Meth. (1981).
- [3] A. Bettini et al., Proc. Conf. Miniaturization in High Energy Phys. Pisa (1980).
- [4] F. Bruyant et al., Nucl. Instr. and Meth. 176 (1980) 409.
- [5] B. Powell et al., to be submitted to Nucl. Instr. and Meth. (1981).
- [6] W. Allison et al., to be submitted to Nucl. Instr. and Meth. (1981).
- [7] D. Crennell et al., Nucl. Instr. and Meth. 158 (1979) 111.
- [8] B. Adeva et al., Phys. Lett. 102B (1981) 285.
- [9] K. Niu, Madison Conference Proceedings (1980).
- [10] R. Schindler et al., Phys. Rev. D 24 (1981) 78.

TABLE CAPTIONS

Table 1 A summary of the fate of all measured charm candidates.

Table 2 Characteristics of the identified charm events. Events 12, 13 and 14 are from proton data.

- n_{ch} = Number of charged prongs at primary vertex.
- n_{π^0} = Number of reconstructed π^0
- n_{γ} = Number of remaining gammas detected at IGD and FGD.
- N_r = Number of secondaries from decay having both momenta and angles determined.
- NDF = Number of degrees of freedom in decay fit.
- NDF = 3; all decay products fully measured.
- NDF = 2; one charged momentum not measured i.e. track not hybridized.
- NDF = 1; two momenta not measured.
- Mass = Reconstructed charm particle mass in MeV/c^2 .
- Length = Decay length in cm.
- L_{proj} = Transverse decay length in μm (x on fig. 7).
- Mom. = Momentum of reconstructed charm particle in GeV/c .
- t = Proper lifetime in units of 10^{-13} s.
- x_F = Feynman x_F ($= 2 P_{11}^*/\sqrt{s}$) at production.
- p_t = Transverse momentum in MeV/c .

TABLE 1

Decay topology	Inside the space box ^(a)	Identified not charm	Identified charm	Under study
C3	49	21	11	17
C5, C7	2	-	-	2
V2 ^(b)	19	10	6	3
V4, V6	7	-	2	5
C1 ^(b)	10	2	1	6
Total	87	33	20	33

(a) The space box is defined by $x < 0.06$ cm and $L < 3$ cm where L is the decay length and x the transverse decay length.

(b) Events with two detected decays.

TABLE 2

Event	$N_{ch} + N_{\pi^0} + N_{\gamma}$	Decay mode	N_{τ}	NDF	Mass (MeV)	Length cm	L_{proj} μm	Momentum (GeV/c)	t 10^{-13} s	x_F	P_t (MeV)	Comment
1	8 0 0	$D^- \rightarrow K^+ \pi^- \pi^-$ C1 not ident. $\Lambda + p\pi^-$	3	3	1867 ± 7 1116	$2.76 \pm .01$.82 \pm .01	138 2973	213.3 ± 2.1 .7 \pm .0	$8.05 \pm .09$.58	389	$t > 1.5 \cdot 10^{-13}$ s
2	12 3 4	$D^- \rightarrow K^+ \pi^- \pi^- \pi^0 \pi^0$ C1	5	3	1863 ± 20	$.88 \pm .01$	402	$43.1 \pm .4$	$12.69 \pm .19$.05	1499	Not identified
3	10 1 5	$D^+ \rightarrow K^- \pi^+ \pi^+ \pi^0$ \bar{D}^0 Mode not ident.	2	1	1867 ± 20	$.19 \pm .01$	127	$8.5 \pm .1$	$13.91 \pm .75$	-.21	602	$P_t = 600 \pm 18$ MeV $t > 10^{-13}$ s
4	8 3 0	$D^0 \rightarrow K^- \pi^+ \pi^0 \pi^0$ $\bar{D}^0 \rightarrow K^+ \pi^+ \pi^- \pi^-$	4 4	3 3	1857 ± 22 1862 ± 9	$.41 \pm .01$.75 \pm .01	129 54	119.0 ± 1.2 78.6 \pm .8	$2.13 \pm .06$ 5.92 \pm .10	.31 .19	643 632	
5	2 2 0	$D^- \rightarrow K^+ \pi^- \pi^-$ $F^+ \rightarrow \pi^+ \pi^0$ $\Lambda + p\pi^-$	3 2	3 3	1840 ± 12 2014 ± 50 1116	$.25 \pm .01$.06 \pm .03 .10 \pm .01	10 < 10 712	181.8 ± 1.8 139.0 ± 1.4 1.0 \pm .0	$.84 \pm .03$.29 \pm .14	.49 .37	1262 1176	Under study: see text Ident. by ionization
6	8 2 0	$\bar{D}^0 \rightarrow K^+ \pi^- \pi^0 \pi^0$ $D^+ \rightarrow \pi^+ K^0$	4 2	3 2	1820 ± 40 1820 ± 100	$.12 \pm .01$.30 \pm .30	97 0	298.1 ± 3.0 26.8 \pm .3	$.24 \pm .02$ 6.79 \pm 6.79	.82 .00	1185 634	
7	10 2 4	$D^- \rightarrow K^+ \pi^- \pi^- \pi^0$ $D^0 \rightarrow K^- \pi^+ \pi^0 \pi^0$	3 3	2 2	1858 ± 31 1880 ± 33	$4.51 \pm .01$.32 \pm .01	203 16	118.7 ± 1.2 76.3 \pm .8	$23.54 \pm .24$ 2.63 \pm .09	.31 .18	354 1123	
8	16 7 14	$\bar{D}^0 \rightarrow K^+ \pi^+ \pi^- \pi^-$ C1	4	3	1850 ± 14	$.35 \pm .01$	84	$80.9 \pm .8$	$1.67 \pm .08$.18	1655	
9	6 2 1	$D^- \rightarrow K^+ \pi^- \pi^-$ $D^0 \rightarrow K^- \pi^+ \pi^0 \pi^0$	3 4	3 3	1865 ± 9 1847 ± 20	$.30 \pm .01$.15 \pm .01	110 70	$35.8 \pm .4$ 43.2 \pm .4	$5.26 \pm .18$ 2.10 \pm .14	.03 .07	983 748	
10	6 3 6	$D^- \rightarrow K^+ \pi^- \pi^- \pi^0 \pi^0$ $D^0 \rightarrow K^- \pi^+ \pi^0$	4 3	2 3	1850 ± 30 1856 ± 11	$.30 \pm .01$ 1.84 \pm .01	127 595	$24.7 \pm .2$ 36.0 \pm .4	$7.50 \pm .26$ 31.61 \pm .36	-.03 .05	1021 325	
11	12 3 5	$D^+ \rightarrow K^- \pi^+ \pi^+ \pi^0$ $\Sigma^- \rightarrow \pi\pi$	4	3	1861 ± 12 1197	$1.34 \pm .01$ 10.1 \pm .01	143 4344	$70.4 \pm .7$ 21.6 \pm .2	$11.81 \pm .15$ 184.17 \pm 1.85	.17 .00	427 942	
12	6 3 3	$D^0 \rightarrow K^- \pi^+ \pi^0 \pi^0$ $F^- \rightarrow K^+ K^+ \pi^-$	5 3	3 3	1840 ± 30 2025 ± 11	$.90 \pm .10$.27 \pm .02	230 48	$49.6 \pm .5$ 43.1 \pm .4	11.14 ± 1.24 4.21 \pm .16	.10 .07	140 541	Ambiguous $\bar{\Lambda}_c^-$
13	12 1 5	$D^- \rightarrow \pi^+ \pi^- \pi^- \pi^0$	4	3	1861 ± 19	$.83 \pm .01$	92	247.4 ± 2.5	$2.08 \pm .03$.68	1054	
14	10 1 3	$D^- \rightarrow K^+ \pi^- \pi^-$	3	3	1859 ± 7	$2.04 \pm .01$	107	$78.1 \pm .8$	$16.17 \pm .18$.19	349	

FIGURE CAPTIONS

- Fig. 1 The NA16 LEBC EHS layout.
- Fig. 2 Typical NA16 charm candidate event in LEBC. Incident 360 GeV proton.
- Fig. 3 The NA16 interaction trigger.
- Fig. 4 Monte-Carlo derived acceptance of the spectrometer for the decay products from D decays (averaged over decay modes) as a function of the x_F of the D meson at production.
- Fig. 5 Reconstructed (a) K^0 and (b) $\Lambda(\bar{\Lambda})$ mass distribution for a sample of strange particle decays.
- Fig. 6 Effective mass distributions of $\gamma\gamma$ samples obtained during the data taking: (a) Both γ 's seen in IGD; (b) both γ 's seen in FGD; (c) All $\gamma\gamma$ combinations.
- Fig. 7 Definition of the event geometrical quantities x, y and L:
- Fig. 8 Effective mass distributions for:
- (a) 3-prong D^\pm decays with Cabibbo preferred (hatched) and Cabibbo unfavoured combinations (4 combinations per event).
 - (b) 3-prong " F^\pm " decays with all $K^+K^-\pi$ combinations (2 combinations per event).
 - (c) 4-prong and 2-prong D^0 decays with Cabibbo preferred (hatched) and Cabibbo unfavoured combinations (note that 4-prong decays have two Cabibbo allowed combinations).
- In all combinations, a fixed number of π^0 is assumed, consistent with overall momentum balance.
- Fig. 9 Corrected lifetime plot for (a) D^\pm sample, (b) D^0 sample.

FIGURE CAPTIONS (Cont'd)

- Fig. 10 (a) D^0 detection efficiency versus x_F (same as fig. 4).
(b) Weighted x_F distribution for all charm decays from the π^-p data. The curves represent $(1 - x_F)^n$, $n = 2, 3$ and 4.
(c) x_F distribution for charm decays from the pp data.

In (b) and (c) neutral decays are represented as hatched. Only decays with $x_F \geq 0.0$ are plotted.

- Fig. 11 Centre of mass rapidity for pair events (a) and single events (b). Note that the geometrical acceptance is close to zero for all $y \leq 0.0$ and high for $y > 0.0$.

- Fig. 12 P_t distribution for all charm decays. Decays with $NDF = 3$ (see table 2) are hatched.

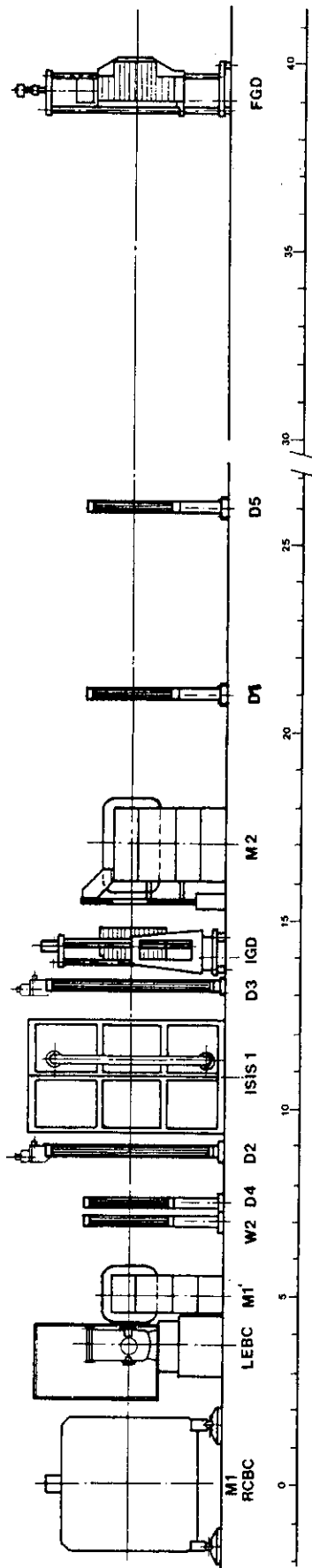
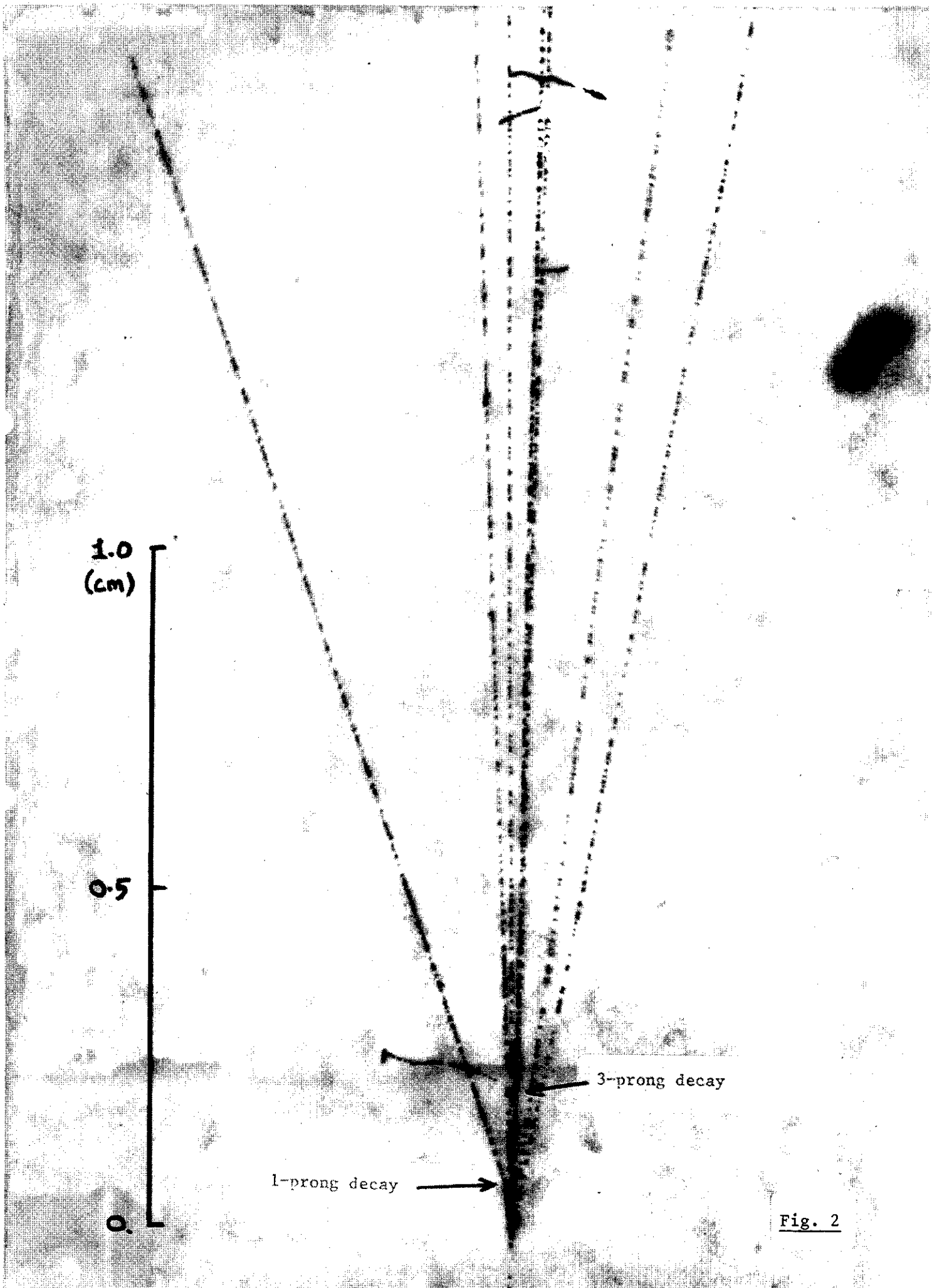


Fig. 1



1.0
(cm)

0.5

0

1-prong decay

3-prong decay

Fig. 2

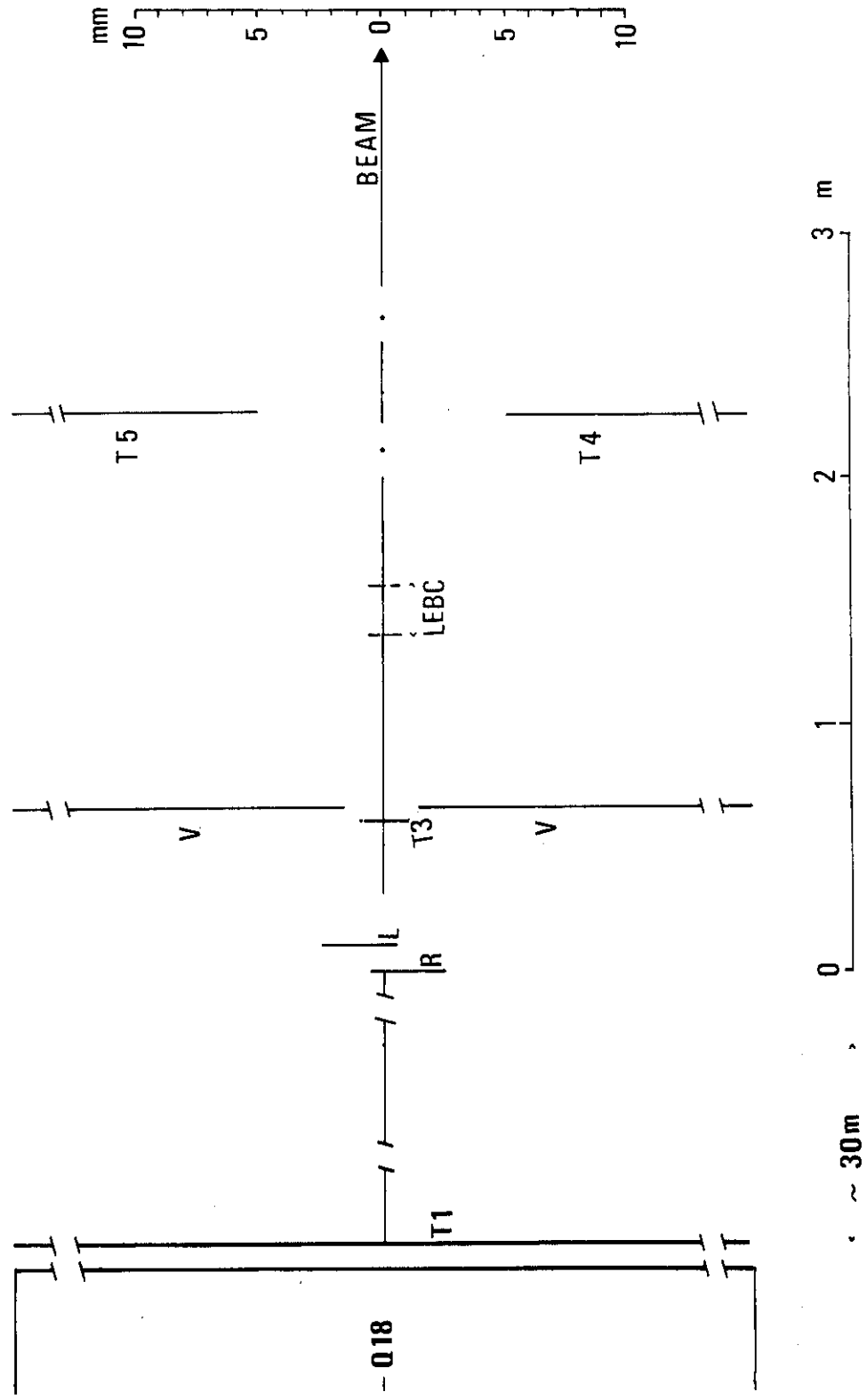
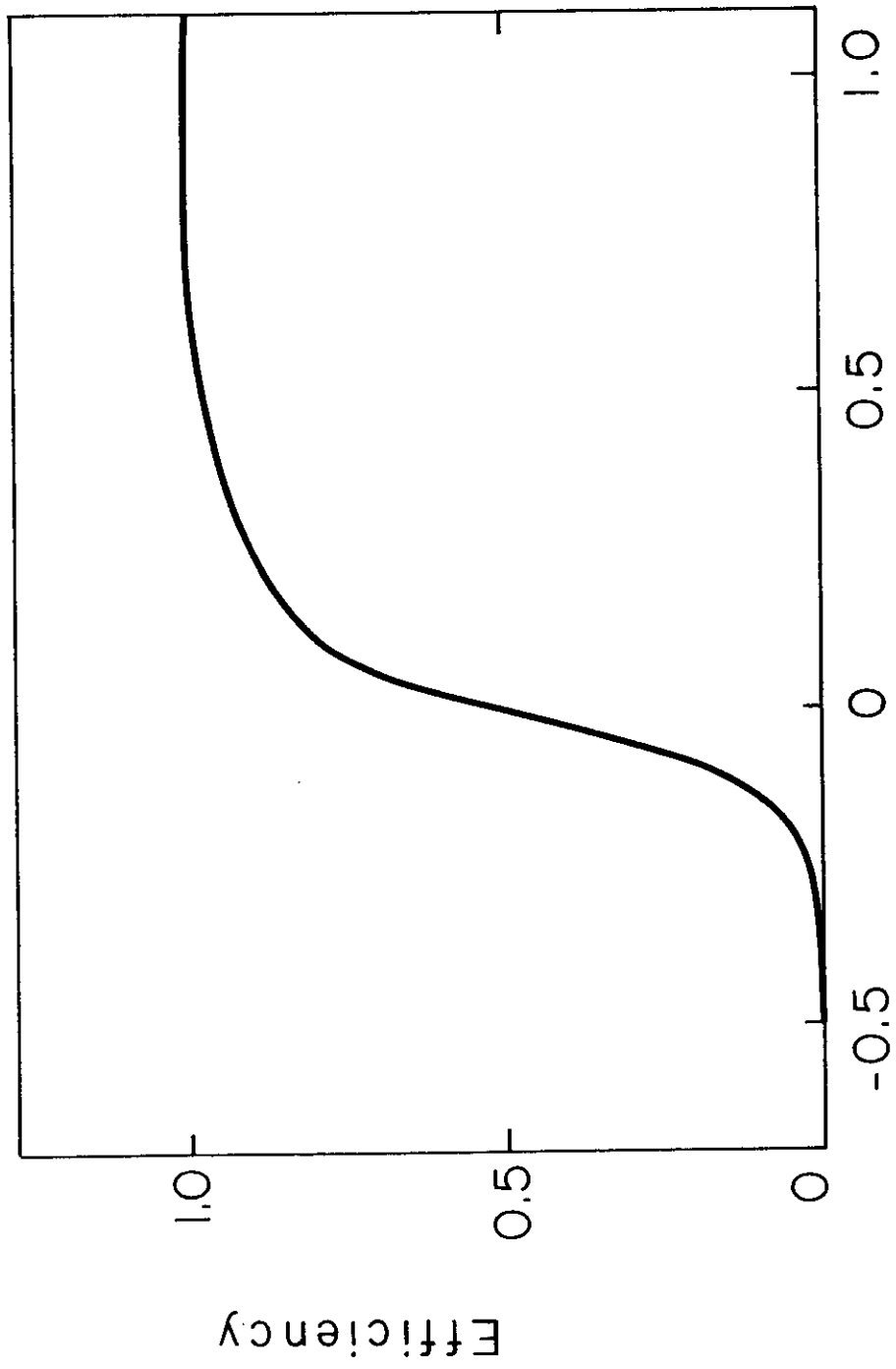


FIG. 3



X_D FIG. 4

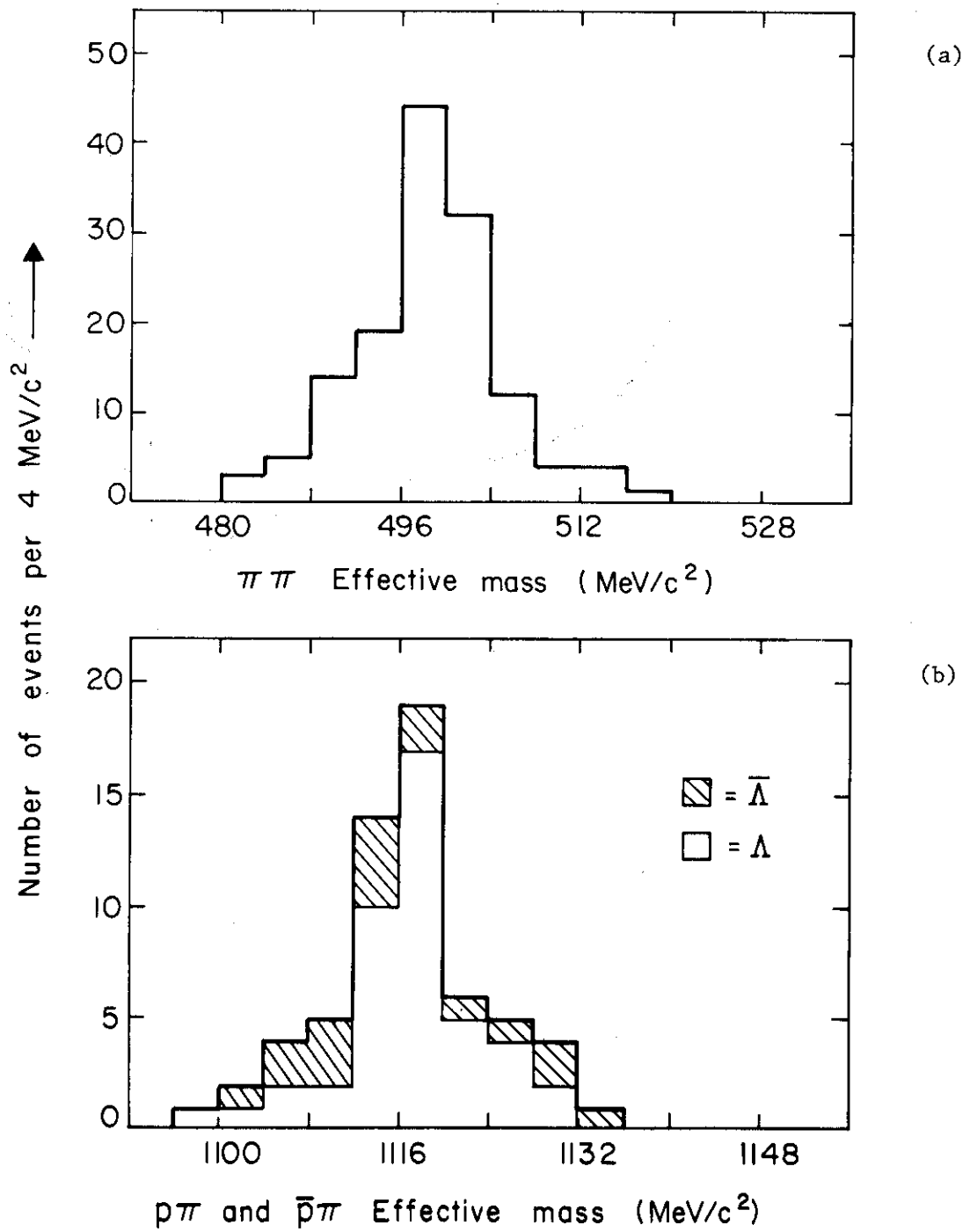


Fig. 5

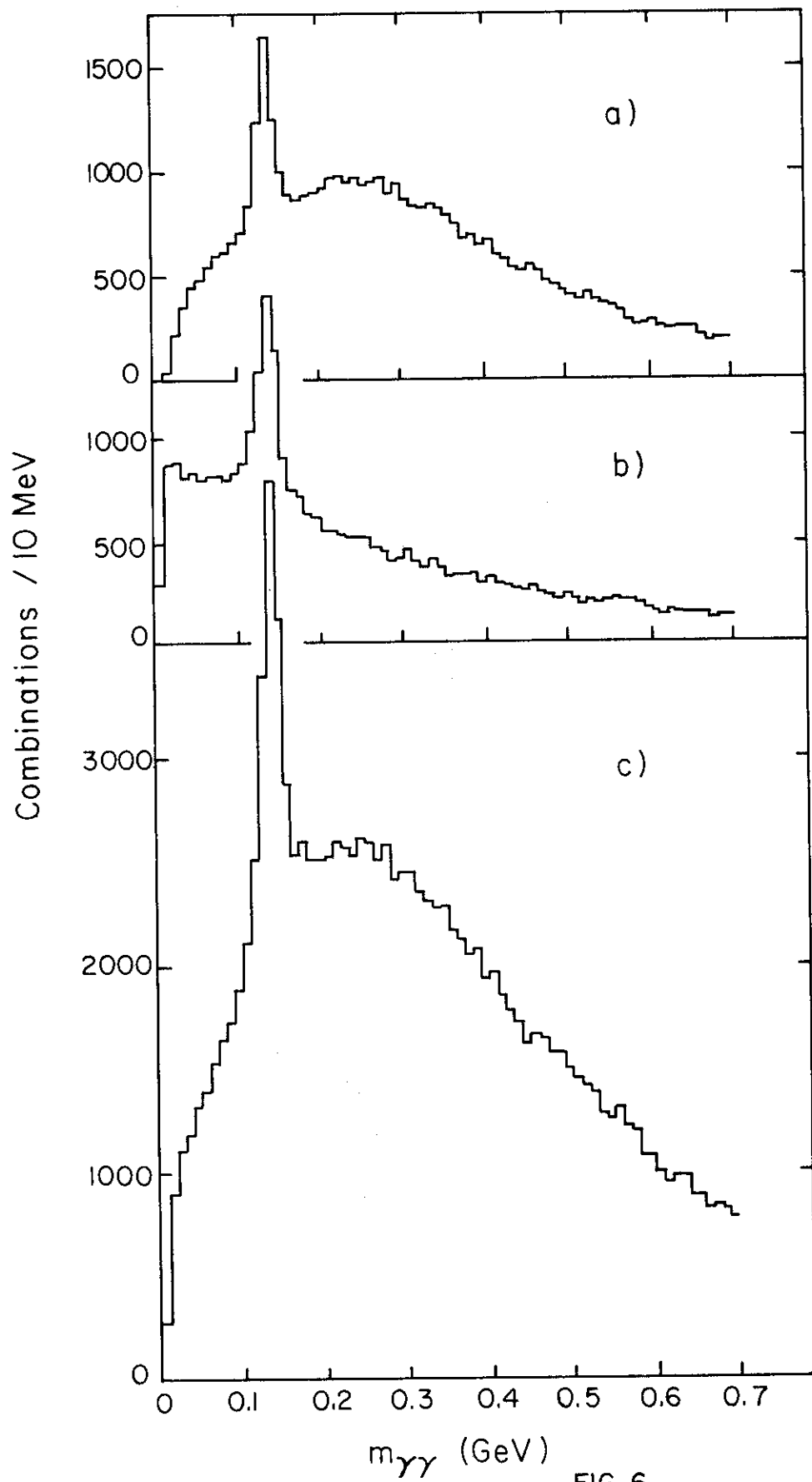


FIG. 6

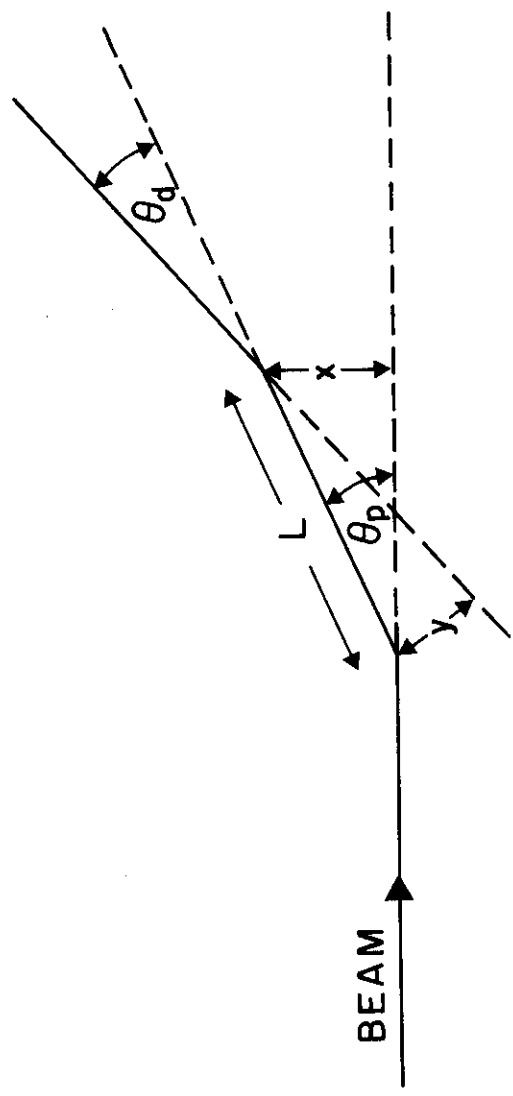


FIG. 7

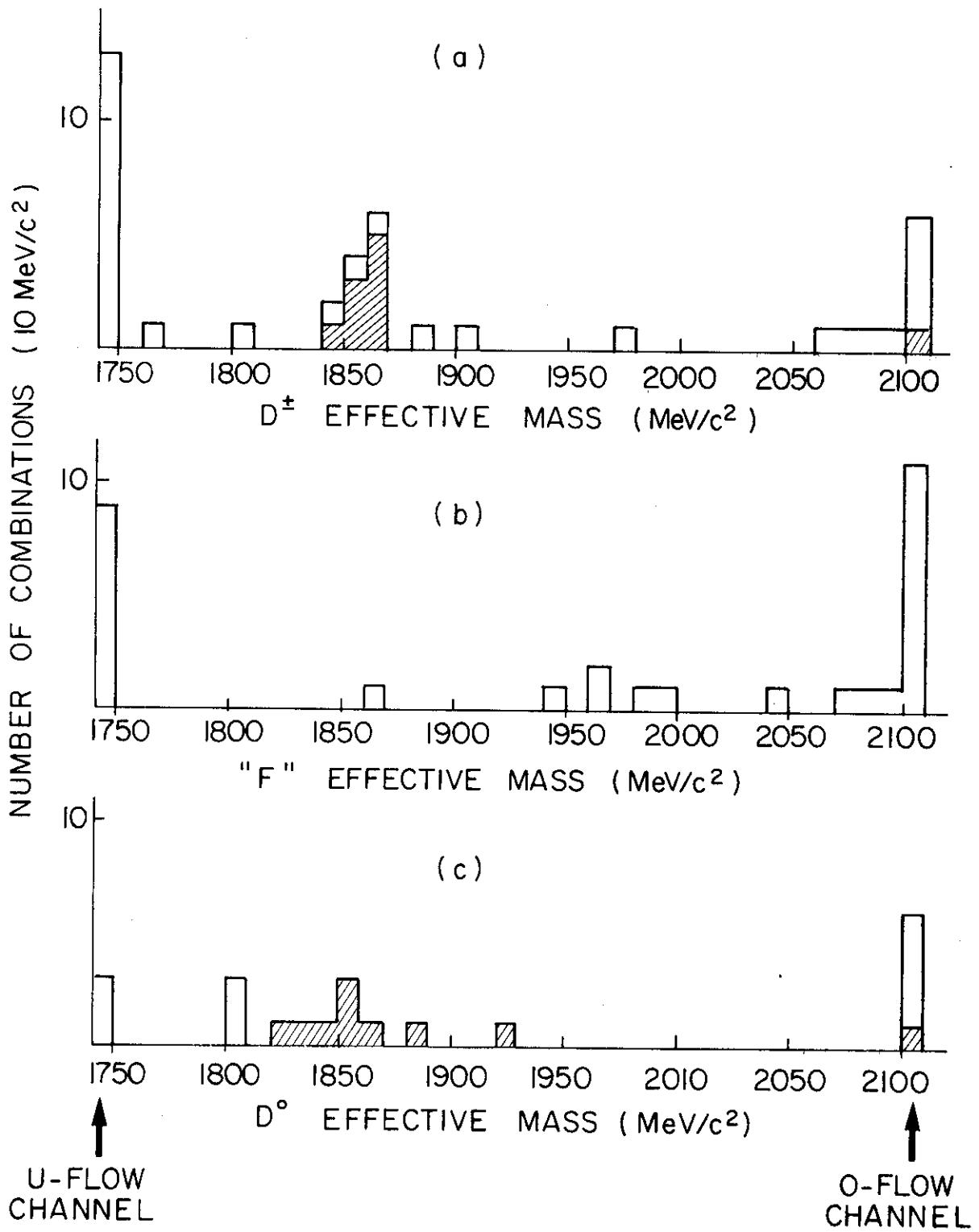


Fig. 8

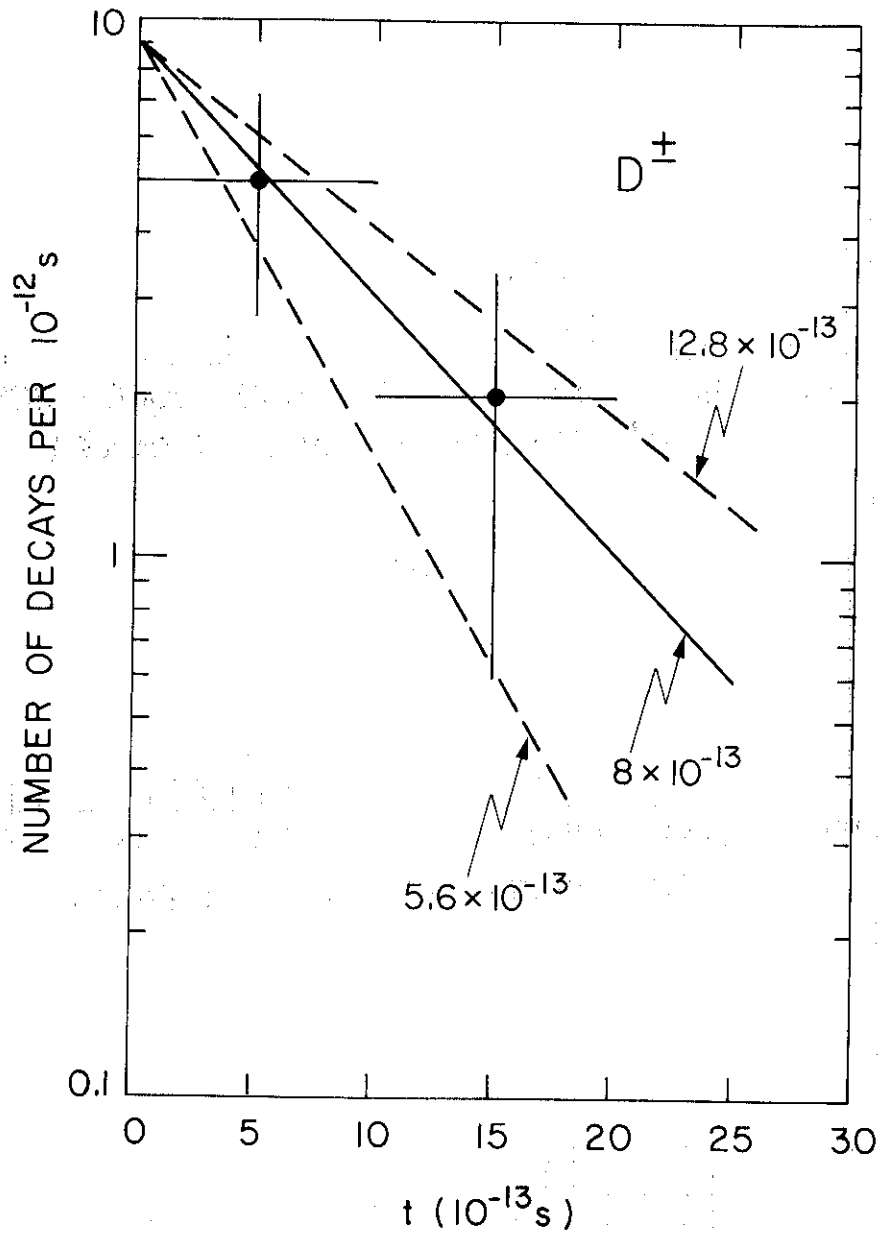


Fig. 9(a)

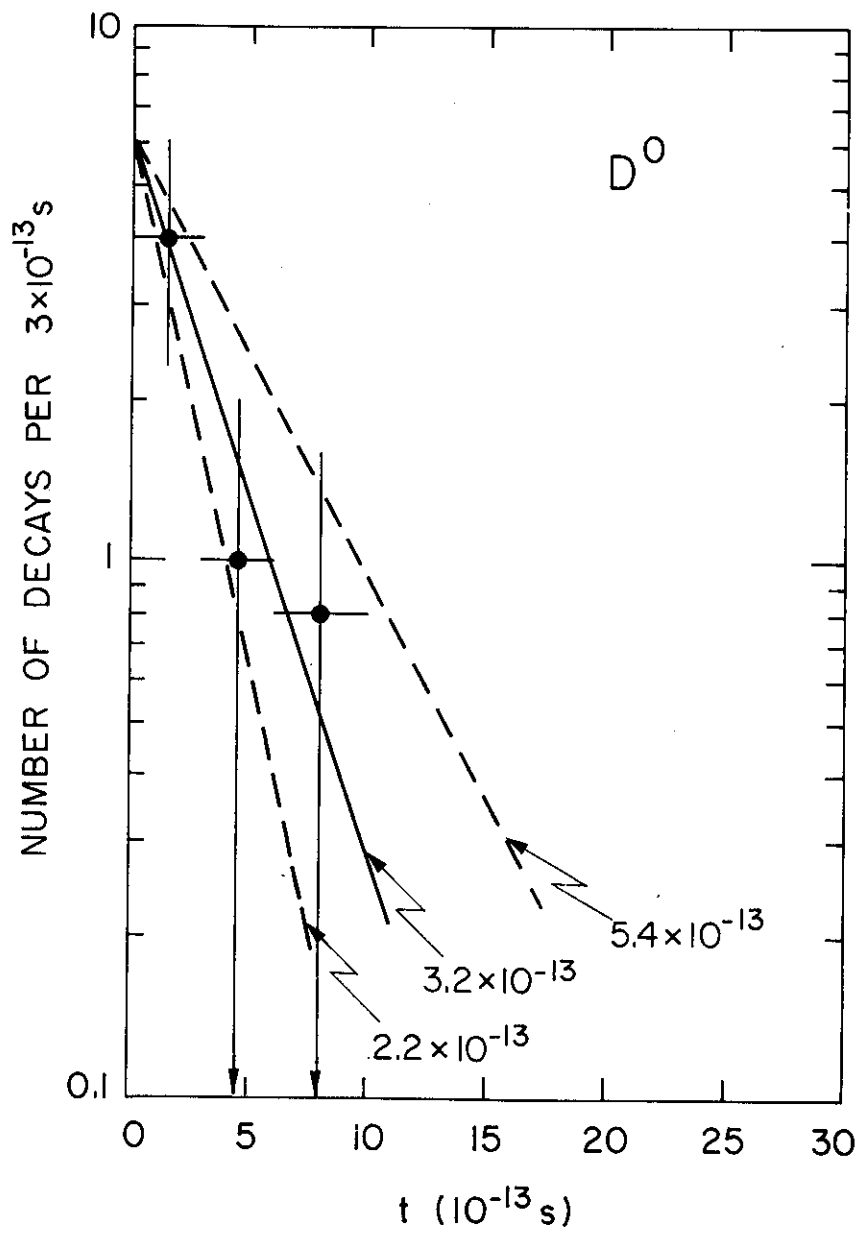


Fig. 9(b)

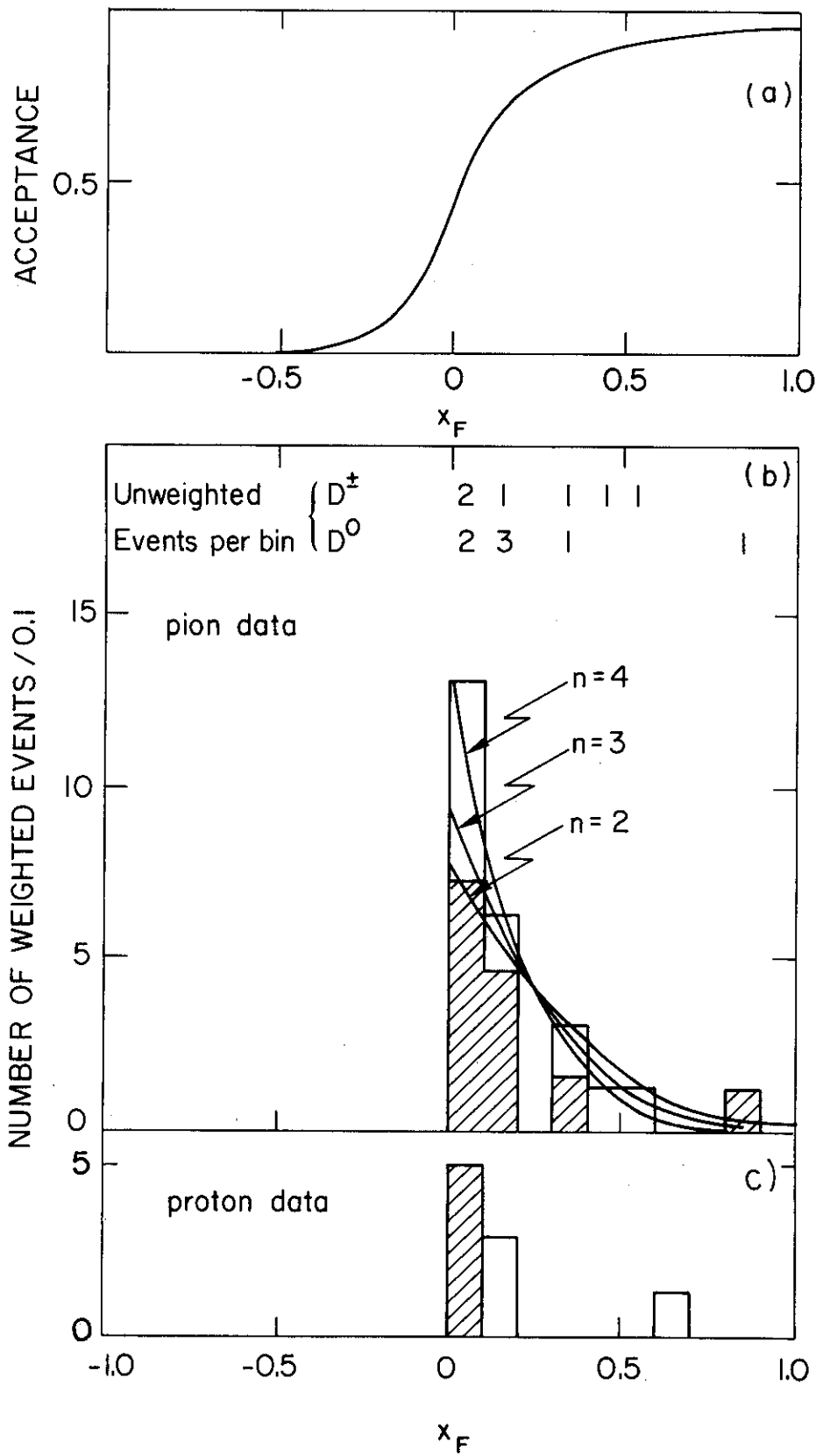


Fig. 10

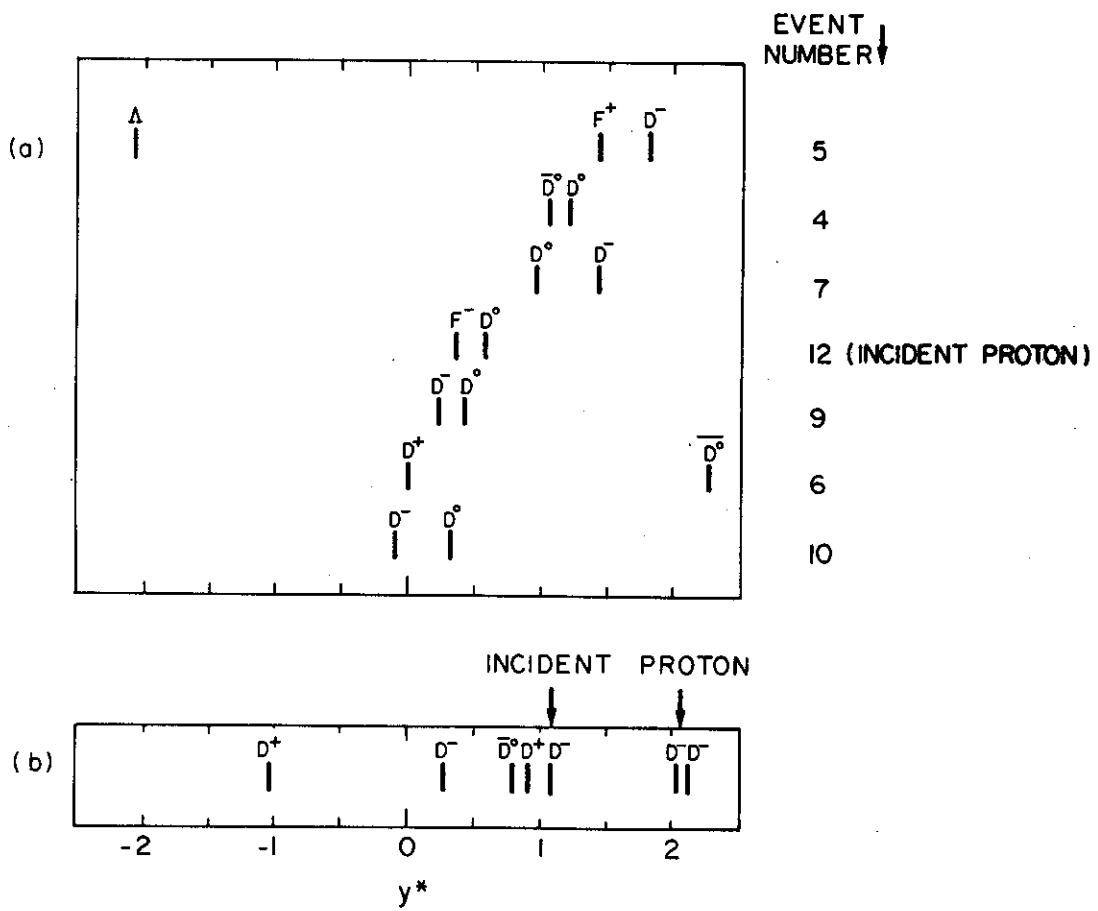


Fig. 11

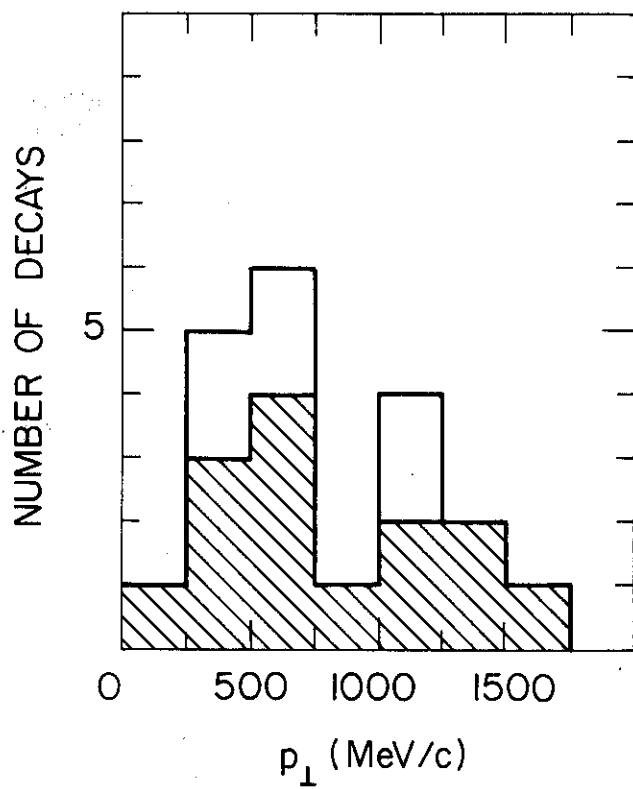


Fig. 12